Room temperature continuous wave operation and characterization of photonic crystal nanolaser on a sapphire substrate

2009 J. Phys. D: Appl. Phys. 42 105113

(http://iopscience.iop.org/0022-3727/42/10/105113)

J. Phys. D: Appl. Phys. **42** (2009) 105113 (5pp) doi:10.1088/0022-3727/42/10/105113

Room temperature continuous wave operation and characterization of photonic crystal nanolaser on a sapphire substrate

M H Shih[1,3], Yi-Chun Yang[1], Yu-Chen Liu[2], Zi-Chang Chang[2], Kung-Shu Hsu[3] and M C Wu[2]

[1] Research Center for Applied Sciences (RCAS), Academia Sinica, 128 Sec. 2, Academia Rd, Nankang, Taipei 11529, Taiwan
[2] Department of Electrical Engineering, National Tsing Hua University (NTHU), 101 Section 2, Kuang-Fu Road, Hsinchu 30013, Taiwan
[3] Department of Photonics, National Chiao Tung University (NCTU), 1001 University Road, Hsinchu 30010, Taiwan

E-mail: mhshih@gate.sinica.edu.tw

Received 5 January 2009, in final form 1 April 2009
Published 30 April 2009
Online at stacks.iop.org/JPhysD/42/105113

Abstract
A compact photonic crystal defect nanocavity was fabricated on a sapphire substrate. Continuous wave lasing at room temperature was achieved with a low threshold power. We characterized the operated mode, quality factor and radiative efficiency for the compact laser. The thermal properties of the nanolaser were also investigated.

(Some figures in this article are in colour only in the electronic version)

1. Introduction

Two-dimensional photonic crystal defect lasers have become a promising technology as novel light sources in dense chip-scale optical systems. There are many reports for photonic crystal defect cavities formed in a suspended membrane [1–7], and most of them can operate only under pulsed pumped conditions. For future integrated photonics, compact continuous wave (CW) operated light sources are required elements; however, there are only a few demonstrations of photonic crystal defect lasers [8–12] that are capable of operation under CW conditions at room temperature. When the size of a photonic integrated system is reduced to the micrometre scale, the sub-micrometre cavity becomes one of the critical elements to fit in the compact platform. The most popular approach is to propose a compact photonic crystal nanocavity in a suspended membrane [7, 13, 14]. These types of nanolasers usually have a higher quality factor (Q) because of their good vertical confinement from the higher index contrast between a semiconductor and air. However, the temperature around the defect region increases by more than 100 K only under pulsed pumped conditions [15]. For a photonic crystal micro-laser operated at room temperature (∼300 K), the threshold will be increased by more than 250%, and very sensitive to temperature since its characteristic temperature is about 40 K [15]. Therefore the operating temperature becomes a critical concern for the membrane compact CW laser. In this paper, we report a sapphire-bonded photonic crystal nanolaser which is capable of room temperature CW operation. Though the photonic crystal microlasers on a sapphire substrate had been demonstrated [11, 16], here we have demonstrated a CW photonic crystal nanolaser in this platform. With better thermal properties, it can operate under higher pumped power and higher environment temperature compared with a similar photonic crystal nanocavity in a suspended membrane. The illustration of a sapphire-bonded photonic crystal nanolaser is shown in figure 1. The low index sapphire substrate here functions as a heat sink for dissipating the heat from the defect region due to its excellent thermal conductivity ($\sim 5 \times 10^{-1}$ W cm^{-1} K^{-1}). With an ultrasmall cavity size, this photonic crystal laser is one of the smallest CW operated lasers [10–12] to date. In

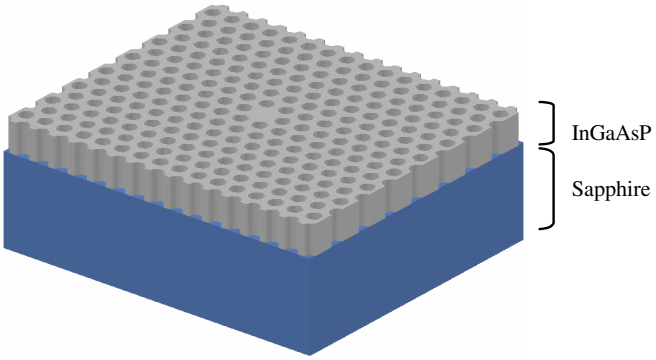

Figure 1. The structure of InGaAsP slab bonded with sapphire substrate.

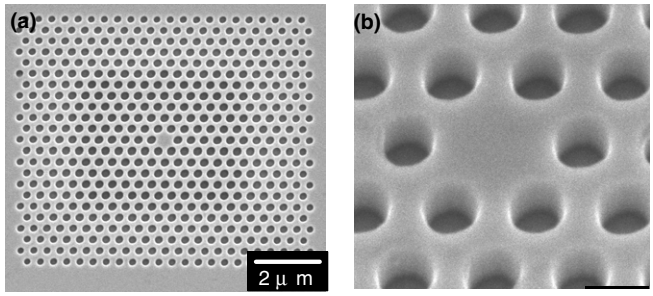

Figure 2. (*a*) SEM image of a D1 sapphire-bonded photonic crystal nanocavity. (*b*) The magnified image of the defect region taken from a 30° angle view.

this paper, we have also studied the optical characteristics and thermal properties of this photonic crystal nanolaser.

2. Fabricated process

These devices were fabricated in a 240 nm thick InGaAsP layer that contains four InGaAsP strained quantum wells (QWs) designed to emit near 1.55 μm at room temperature. These InGaAsP layers were deposited by metal–organic chemical vapor deposition (MOCVD) on an InP substrate. The wafer was then bonded to a sapphire substrate and annealed in a H_2 chamber at 480 °C. The InP substrate was removed by a wet etching procedure with HCl solution. After the wafer bonding step, the photonic crystal cavities were fabricated in the InGaAsP layer. A silicon nitride (SiN_x) mask was deposited in a plasma enhanced chemical vapor deposition (PECVD) system and a 5% polymethylmethacrylate (PMMA) resist was spin coated on the top of the SiN_x layer. The photonic crystal cavities were defined by electron beam lithography, and the photonic crystal patterns were transferred into the SiN_x mask using a reactive ion etch (RIE) system with CHF_3/O_2 mixture. The pattern was transferred into the InGaAsP layer using an inductively coupled plasma (ICP) system with a $CH_4/Cl_2/H_2$ mixture. The mask was removed at the end of the fabrication.

3. Characterization of the sapphire-bonded photonic crystal nanolaser

The D1 photonic crystal nanocavities were formed by a single hole defect in the triangular photonic crystal lattices. We label this cavity D1 because of the one missing hole from the hexagon photonic crystal lattices. The cavity is surrounded by more than 10 periods of photonic crystal lattice cladding which support enough in-plane confinement for the CW nanolaser [11]. The laser cavities were optically pumped at room temperature using an 850 nm diode laser at normal incidence. The pumped spot was focused by a 100× objective lens to a spot approximately 1.5 μm in diameter. The output power was collected from the top of the cavities by a multi-mode fibre which was connected to an optical spectrum analyzer. Figure 2(*a*) is a scanning electron microscope (SEM) image of a photonic crystal nanocavity with a lattice constant of 422 nm, and figure 2(*b*) is a magnification of the defect region taken from a 30° angle view. The size of this photonic crystal nanocavity is only about 580 nm in diameter.

Three-dimensional (3D) plane-wave expansion (PWE) and finite-difference time-domain (FDTD) methods were used to simulate this sapphire-bonded photonic crystal nanocavity. Figure 3(*a*) is the band diagram of the photonic crystal lattices on a sapphire substrate from 3D PWE calculation. To prevent the power leakage out of the InGaAsP slab, only the region below the light-line (thick black line) will be considered. The first band-gap region is from 0.26 to 0.33 in normalized frequency (a/λ). Figure 3(*b*) shows the calculated spectrum (blue solid line) of the nanocavity from the FDTD simulation. The high-Q defect mode (A) is shown at the normalized frequency of 0.28. Figure 3(*c*) shows the top view of the H_z field profile of the defect mode from the FDTD simulation. The estimated mode volume of the nanocavity is only $0.023\ \mu m^3 \sim 1.5\,(\lambda/2n)^3$, where n is the refractive index of the InGaAsP slab.

Figure 4(*a*) shows a lasing spectrum of a D1 sapphire-bonded photonic crystal cavity pumped at twice the threshold power under room temperature CW conditions. The lasing wavelength is 1587.6 nm. The side-mode suppression-ratio (SMSR) of this laser is approximately 17 dB, which is good for optical communication. Figure 4(*b*) shows the light-in light-out curve (L–L curve) of the nanolaser. The lasing threshold occurred at 0.85 mW in incident power. The effective threshold power is only 35 μW after estimating the material absorption and surface reflectivity of the cavity structure.

The polarization of the operated mode is also characterized with a linear polarizer. The measured polarization curve of the lasing signal is shown in figure 5. The polarization ratio can be defined by the formula

$$\text{Polarization degree} = \frac{I_{\max} - I_{\min}}{I_{\max} + I_{\min}},$$

where I is the signal intensity. We obtained approximately 90% polarization from the lasing signal. The nanolaser has the definite polarization direction that indicates the lasing mode oscillates along the particular in-plane direction. It confirms the lasing operation of the defect mode and the mode profile from the FDTD simulation, since the polarization degree of the photonic crystal band edge mode is usually relatively low. With

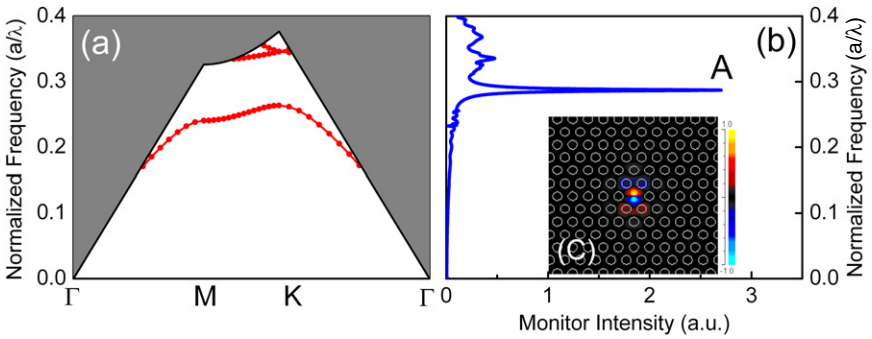

Figure 3. The simulated results for the photonic crystal nanocavity on a sapphire substrate. (*a*) The band diagram (red solid dotted line) of the photonic crystal lattices from the PWE method. The thick black curve is the light-line. (*b*) The FDTD simulated spectrum (blue solid line) for this nanocavity. The defect mode at a normalized frequency (a/λ) of 0.28 is labelled mode A. (*c*) The top view of the H_z field profile of mode A which is obtained from the FDTD simulation.

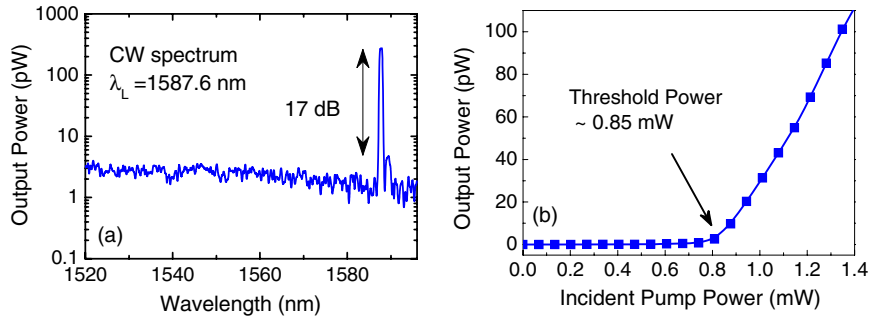

Figure 4. (*a*) The lasing spectrum from a D1 sapphire-bonded photonic crystal cavity under CW pumped conditions at room temperature. Its lasing wavelength is 1587.6 nm and SMSR is about 17 dB. (*b*) The light-in light-out curve of this D1 laser cavity. The incident threshold power is about 0.85 mW.

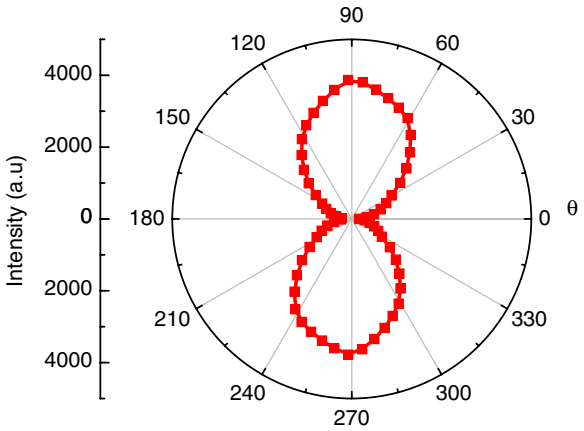

Figure 5. The measured polarization curve of the lasing mode from a D1 sapphire-bonded photonic crystal cavity under room temperature CW conditions.

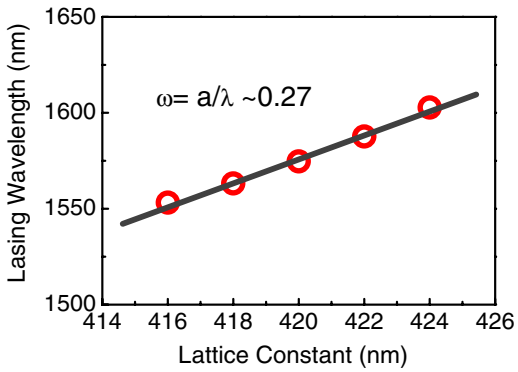

Figure 6. The lasing wavelength versus the lattice constant of photonic crystal nanocavity. The normalized frequency of this lasing mode is approximately 0.27.

a photonic crystal cavity, we can tune the resonant wavelength lithographically. Figure 6 shows the lasing wavelength versus the lattice constants of the nanocavities. The linearity of the data indicates that these cavities are all lasing in the same defect mode with a normalized frequency (a/λ) of 0.27. The lasing wavelength of the cavities in these data shifts by approximately 69 nm by increasing the lattice constant by 8 nm. The wavelength tuning rate is about 8.6 nm for a 1 nm variation in lattice constant.

4. Quality factor and radiative efficiency of the CW photonic crystal nanolaser

From the threshold power, the parameters of the InGaAsP QWs and the geometrical parameters of the cavities, we can estimate the quality factor (Q) and optical characteristics of the photonic crystal nanocavities with a simple model [11]. The threshold power of a semiconductor laser can be attributed into three parts, surface recombination, spontaneous radiative recombination and Auger recombination, which are proportional to the carrier density (n), the square of

Table 1. Parameters used for characterizing the sapphire-bonded photonic crystal nanolasers.

Parameters	Value
Surface recombination velocity (v_s)	10^4 cm s^{-1}
Radiative recombination coefficient (B)	1.6×10^{-10} cm^3 s^{-1}
Auger recombination coefficient (C)	3.0×10^{-29} cm^6 s^{-1}
Modal gain (G_0) of InGaAsP QWs	76 cm^{-1}
InP index of refraction	3.17
Photonic crystal cavity confinement factor	0.15
Cavity size in diameter	580 nm
Volume of active region	0.068 μm^3

the carrier density and the cubic of the carrier density, respectively (equation (1)) [17, 18]. The incident optical power was converted into an effective current (I_{elec}). The recombination currents due to surface recombination (I_{sr}), radiative recombination (I_{sp}) and Auger recombination (I_{auger}) were also determined with the coefficients A, B and C in [17]:

$$I_{\text{elec}} = I_{\text{sr}}(n) + I_{\text{sp}}(n^2) + I_{\text{Auger}}(n^3). \tag{1}$$

Then the modal gain can be determined for a QW laser using [19]

$$G = G_0 \ln\left(\frac{I_{\text{elec}} - I_{\text{sr}}}{I_{\text{tr}}}\right), \tag{2}$$

where G_0 is about 76 cm^{-1} for our photonic crystal lasers and I_{tr} is the transparency current for our QW. G_0 was determined from material gain measurements made on broad area lasers with the same active region as in [19] and then the confinement factor was calculated from a simple finite difference algorithm. The quality factors of the cavities were obtained from the threshold modal gains using

$$Q = \frac{2\pi n_{\text{InP}}}{\lambda G_{\text{th}}}, \tag{3}$$

where $n_{\text{InP}} = 3.17$ and G_{th} is the threshold modal gain.

By solving the carrier density, we can obtain the recombination currents of three components. The radiative efficiency of these compact CW nanolasers can be estimated with the following formula [18]:

$$\eta_{\text{sp}} = \frac{Bn}{A + Bn + Cn^2}. \tag{4}$$

Table 1 lists the parameters we used to analyse this photonic crystal nanolaser, and the optical characteristics of the device are provided in table 2. We obtained a quality factor of 320 for the nanocavity which is close to the simulated value from the FDTD. The radiative efficiency is approximately 0.18 after substituting the carrier density into equation (4). Because of the ultrasmall cavity size and the mode distribution, most of the carriers are consumed in surface recombination and Auger recombination for this nanocavity. However, the efficiency could be increased by the further designed photonic crystal cavities.

Table 2. Characterization of the sapphire-bonded photonic crystal nanolasers.

Characteristics of the sapphire-bonded photonic crystal nanolaser	Value
Cavity mode volume	0.023 μm^3 $\sim 1.5(\lambda/2n)^3$
Side-mode suppression-ratio (SMSR)	17 dB
Incident threshold power (mW)	0.85
Estimated Q value	320
Radiative efficiency (η_{sp})	0.18

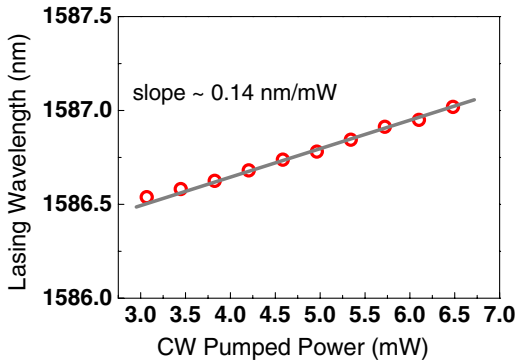

Figure 7. The lasing wavelength of the photonic crystal nanolaser versus the pumped power. The slope, $\frac{\Delta\lambda}{\Delta P}$ is about 0.14 nm mW^{-1}.

5. Thermal properties of the CW photonic crystal nanolasers

One of the advantages of the sapphire-bonded photonic crystal lasers is better thermal properties because of the excellent heat dissipation with the sapphire substrate. In order to characterize the thermal impedance of the nanocavity, we monitored the shift of the lasing wavelength above the threshold by varying the pumped power. Figure 7 shows the lasing wavelength of a D1 photonic crystal laser versus the pumped power. The rate at which the lasing wavelength shifts with increasing pumped power, $\frac{\Delta\lambda}{\Delta P}$ is approximately 0.14 nm mW^{-1}. The thermal impedance of this bonded photonic crystal cavity can be determined by the following equation [17, 20]:

$$\frac{1}{R_{\text{Th}}} = \frac{\Delta T}{\Delta P} = \frac{\Delta\lambda}{\Delta P} \cdot \frac{\Delta T}{\Delta\lambda}, \tag{5}$$

where R_{Th} is the thermal resistance, ΔT is the temperature change, ΔP is the absorbed power from optical pumping and $\Delta\lambda$ is the lasing wavelength shift of the device. The lasing wavelength shift due to temperature changes, $\frac{\Delta\lambda}{\Delta T}$, is about 0.05 nm K^{-1} [15]. After substituting these two values into equation (5), we obtained a thermal impedance of this photonic crystal nanolaser that is approximately 2.8 K mW^{-1}. The value for this photonic crystal nanolaser is larger than the values reported for vertical-cavity surface-emitting lasers (VCSELs), of about 1 K mW^{-1} [20, 21]; however it is much smaller than the reported value, 10^6 K W^{-1}, from a photonic crystal nanolaser in a suspended membrane [12]. We attributed this lower value to the fact that the sapphire substrate has much better thermal conductivity than air. Although a higher Q might be obtained from a suspended membrane cavity,

the sapphire-bonded cavity still has reasonable Q and better thermal properties. Therefore this sapphire-bonded photonic crystal nanolaser can be an excellent CW nano-scale light source for future photonic integrated circuits.

6. Summary

In short, we have demonstrated a sapphire-bonded photonic crystal nanolaser under CW operating conditions at room temperature. The CW nanolaser has ultrasmall size, excellent heat dissipation, low threshold and a high SMSR. We characterized the quality factor and radiative efficiency for the nanolaser. The thermal impedance of the nanocavity was also evaluated from the lasing wavelength shift under different pumped powers.

Acknowledgments

The authors would like thank the Center for Nano Science and Technology and Professor P T Lee at the National Chiao Tung University (NCTU) for the fabrication facilities. This study is based on research supported by the National Science Council (NSC) of ROC, Taiwan, under Grant No NSC-96-2112-M-001-037-MY3 and by the Grant of the Academia Sinica, Taiwan.

References

[1] Painter O, Lee R K, Scherer A, Yariv A, O'Brien J D, Dapkus P D and Kim I 1999 Two-dimensional photonic band-gap defect mode laser *Science* **284** 1819–21

[2] Lee P T, Cao J R, Choi S J, Wei Z J, O'Brien J D and Dapkus P D 2002 Room-temperature operation of VCSEL-pumped photonic crystal lasers *IEEE Photon. Technol. Lett.* **14** 435–7

[3] Hennessy K, Reese C, Badolato A, Wang C F, Imamoglu A, Petroff P M, Hu E, Jin G, Shi S and Prather D W 2003 Square-lattice photonic crystal microcavities for coupling to single InAs quantum dots *Appl. Phys. Lett.* **83** 3650–2

[4] Akahane Y, Asano T, Song B S and Noda S 2003 High-Q photonic nanocavity in a two-dimensional photonic crystal *Nature* **425** 944–7

[5] Monat C *et al* 2003 Two-dimensional hexagonal-shaped microcavities formed in a two-dimensional photonic crystal on an InP membrane *J. Appl. Phys.* **93** 23–31

[6] Altug H and Vuckovic J 2005 Photonic crystal nanocavity array laser *Opt. Express* **13** 8819–28

[7] Ee H S, Jeong K Y, Seo M K, Lee T H and Park H G 2008 Ultrasmall square-lattice zero-cell photonic crystal laser *Appl. Phys. Lett.* **93** 011104

[8] Hwang B J K, Ryu H Y, Song D S, Han I Y, Park H K, Jang D H and Lee Y H 2000 Continuous room-temperature operation of optically pumped two-dimensional photonic crystal lasers at 1.6 μm *IEEE Photon. Technol. Lett.* **12** 1295–7

[9] Song B S, Asano T, Akahane Y, Tanaka Y and Noda S 2004 Transmission and reflection characteristics of in-plane hetero-photonic crystals *Appl. Phys. Lett.* **85** 4591–3

[10] Nomura M, Iwamoto S, Watanabe K, Kumagai N, Nakata T, Ishida S and Arakawa Y 2006 Room temperature continuous-wave lasing in photonic crystal nanocavity *Opt. Express* **14** 6308–15

[11] Shih M H, Kuang W, Yang T, Bagheri M, Wei Z J, Choi S J, Lu L, O'Brien J D and Dapkus P D 2006 Experimental characterization of the optical loss of sapphire-bonded photonic crystal laser cavities *IEEE Photon. Technol. Lett.* **18** 535–7

[12] Nozaki K, Kita S and Baba T 2007 Room temperature continuous wave operation and controlled spontaneous emission in ultrasmall photonic crystal nanolaser *Opt. Express* **15** 7506–751

[13] Nozaki K and Baba T 2006 Laser characteristics with ultimate-small modal volume in photonic crystal slab point-shift nanolasers *Appl. Phys. Lett.* **88** 211101

[14] Kim S H, Choi J H, Lee S K, Kim S H, Yang S M, Lee Y H, Seassal C, Regrency P and Viktorovitch P 2008 Optofluidic integration of a photonic crystal nanolaser *Opt. Express* **16** 6515

[15] Lee P T, Cao J R, Choi S J, Wei Z J, O'Brien J D and Dapkus P D 2002 Operation of photonic crystal membrane lasers above room temperature *Appl. Phys. Lett.* **81** 3311

[16] Shih M H, Bagheri M, Mock A, Choi S J, O'Brien J D, Dapkus P D and Kuang W 2007 Identification of modes and single mode operation of sapphire-bonded photonic crystal lasers under continuous-wave room temperature operation *Appl. Phys. Lett.* **90** 121116

[17] Coldren L A and Corzine S W 1995 *Diode Lasers and Photonic Integrated Circuits* (New York: Wiley)

[18] Agrawal G P and Dutta N K 1993 *Semiconductor Lasers* (New York: Van Nostrand Reinhold)

[19] Mathur A and Dapkus P D 1996 Fabrication, characterization and analysis of low threshold current density 1.55 μm-strained quantum-well lasers *IEEE J. Quantum Electron.* **32** 222

[20] Krishnamoorthy A V, Goossen K W, Chirovsky L M F, Rozier R G, Chandramani P, Hobson W S, Hui S P, Lopata J, Walker J A and D'Asaro L A 2000 16 $\times$ 16 VCSEL array flip-chip bonded to CMOS VLSI circuit *IEEE Photon. Technol. Lett.* **12** 1073

[21] Mathine D L, Nejad H, Allee D R, Droopad R and Maracas G N 1996 Reduction of the thermal impedance of vertical-cavity surface-emitting lasers after integration with copper substrates *Appl. Phys. Lett.* **69** 463